Weierstraß-Institut

für Angewandte Analysis und Stochastik

im Forschungsverbund Berlin e. V.

Preprint ISSN 0946 – 8633

Interface morphologies in liquid/liquid dewetting

Konstantina Kostourou[1], Dirk Peschka[2], Andreas Münch[3],

Barbara Wagner[2], Stephan Herminghaus[1], Ralf Seemann[1,4]

submitted: November 2, 2010

[1] Max Planck Institute for Dynamics
and Self-Organization
Bunsenstraße 10
37073 Göttingen, Germany

[2] Weierstrass Institute for
Applied Analysis and Stochastics
Mohrenstraße 39
10117 Berlin, Germany

[3] Mathematical Institute
University of Oxford
24-29 St. Giles'
Oxford OX1 3LB, UK

[4] Experimental Physics
Saarland University
PO Box 151 150
Saarbrücken, Germany

No. 1560
Berlin 2010

2010 *Mathematics Subject Classification.* 76A20, 76D08, 35R35, 76-05.

Key words and phrases. thin films, polymer-polymer dewetting, lubrication theory, numerical solution.

We acknowledge financial support by the European Community through the "Marie-Curie Actions" under Contract MRTN-CT-2004-504052 [POLYFILM] and the Priority Programs SPP 1164 [Micro- and nanofluidics] and SPP 1506 [Transport processes at fluid interfaces] of the German Science Foundation.

Edited by
Weierstraß-Institut für Angewandte Analysis und Stochastik (WIAS)
Mohrenstraße 39
10117 Berlin
Germany

Fax: +49 30 2044975
E-Mail: preprint@wias-berlin.de
World Wide Web: http://www.wias-berlin.de/

Abstract

The dynamics and morphology of a liquid polystyrene (PS) film on the scale of a hundred nanometer dewetting from a liquid polymethylmethacrylate (PMMA) film is investigated experimentally and theoretically. The polymers considered here are both below their entanglement lengths and have negligible elastic properties. A theoretical model based on viscous Newtonian flow for both polymers is set up from which a system of coupled lubrication equations is derived and solved numerically. A direct comparison of the numerical solution with the experimental findings for the characteristic signatures of the cross-sections of liquid/air and liquid/liquid phase boundaries of the dewetting rims as well as the dewetting rates is performed and discussed for various viscosity ratios of the PS and PMMA layers.

1 Introduction

Understanding the dewetting properties of liquid films has been a frequently studied problem in recent years due to their importance in numerous scientific and technological processes. One major focus of interest has been to understand the stability of thin liquid films [1, 2, 3]. Various rupture mechanisms and dynamic phenomena on solid substrates have been the subject of theoretical and experimental studies[4, 5, 6, 7]. Once holes are generated, an important focus was to understand the dynamics and morphology of thin films dewetting from hydrophobic substrates [8, 9, 10, 11, 12, 13, 14]. Thin polymer films with reasonably high molecular weight have proven to be ideal model systems for this kind of studies due to their low vapor pressure, easily tunable viscosity, and their commercial availability with very low polydispersity. While most studies so far have explored the dewetting of thin liquid films on rigid substrates, the more complex situation of a liquid dewetting on a deformable, liquid substrate has received less attention in the past.

The difficulty of liquid/liquid systems is that not only the polymer/air interface has to be considered, but even more importantly the deformation of and the boundary conditions at the (liquid) substrate/air and the (liquid) substrate/liquid interface. Only a few experimental studies exist on dewetting and film instabilities of liquid/liquid systems. But the deformation of the liquid/liquid interface is probed either directly by neutron reflectometry without considering the liquid/air interface [15] or indirectly by the resulting deformation of the liquid/air interface probed by scanning force microscopy [16]. Another group studied the breakup and the hole growth of a liquid/liquid system where the viscosity of one of the liquids is much larger than the viscosity of the other liquid [17]. The hole growth has also been studied in the past but only in a very special case, where the resulting dewetting morphologies are all coated with a thin layer of the underlying liquid [18].

The shape of an underlying liquid polymethylmethacrylate (PMMA) substrate and the liquid polystyrene (PS) rim profile dewetting from this substrate has been studied first in the pioneering work of the group of G. Krausch [19, 20]. They found a characteristic rim shape, depending on the relative viscosity of the two liquids. They also found a behavior of the dewetting dynamics for different chain length of the substrate that was claimed to be in agreement with an earlier study [21]. Further experimental work has been performed by Qu et al. [22] for PS dewetting from PMMA of high molecular weight.

All of these studies consider polymers of molecular weight that are well above their entanglement length and the elastic properties of the polymer melts are very likely to significantly influence morphology and dynamics of the dewetting process. One aim of this study is to keep the molecular weight of both polymers (here PS and PMMA) below or at their entanglement lengths, so that elastic properties of the polymers can be neglected. This allows for a theoretical description based on viscous Newtonian flow for both polymers.

Apart from the early and fundamental work by Brochard-Wyart et al. [21] on liquid/liquid dewetting, only a few groups have been studying this system theoretically. Here we point to the works by Pototsky et al. [23, 24], Fisher and Golovin [25, 26], and by Bandyopadhyay et al. [27, 28]. However, direct comparisons to experimental results are not available, and this is a further aim of this study. We will compare characteristic features such as dewetting rates, the morphology of the dewetting rims and the underlying liquid/liquid interface, and systematically explore how they depend on the ratios of the viscosities of the used polymers.

2 Materials and methods

The polymer employed in our experiments as the dewetting liquid is atactic polystyrene purchased from Polymer Standards Service (Mainz, Germany) with a monodispersity of $\mathrm{M}_w/\mathrm{M}_n = 1.04$ and a molecular weight of $\mathrm{M}_w = 17.4$ kg/mol (17k). This molecular weight is just below the entanglement length and thus the polymer melt can be approximately treated as a Newtonian liquid [5, 29]. The viscosity of PS (17k) at $170\,^{\circ}\mathrm{C}$ is $\mu_{\mathrm{PS,17k}} \approx 0.2$ kPa· s. The surface tension of PS in air is $\gamma_{\mathrm{PS/air}} = 32 \pm 2$ mN/m. Thin PS films in the range of 35 - 50 nm were prepared by spin-coating polystyrene solved in toluene onto a freshly cleaved mica sheet. The solidified polystyrene film was subsequently floated on Millipore™water and picked up with the viscous substrate.

As viscous substrates, thin PMMA layers of about $200\,nm$ thickness were prepared by spin coating a toluene solution on previously cleaned silicon (Si) substrates, cut in the <100> direction. The PMMA we used was purchased from Polymer Standards Service (Mainz, Germany). An important physical property of PMMA that makes it suitable for our studies is its immiscibility with PS and its low contact angle on silicon, such that it constitutes a stable substrate for the PS film. The viscosity was varied by changing the molecular chain length and temperature. For the experimental results presented here, three different PMMA molecular weights were typically used, all below or around the entanglement length: 4.2 kg/mol (4k), 10.1 kg/mol (10k), 14.1 kg/mol (14k) with a monodispersity of $\mathrm{M}_w/\mathrm{M}_n = 1.04$, and viscosities at $170\,^{\circ}\mathrm{C}$ of $\mu_{\mathrm{PMMA,4k}} \approx 6\,\mathrm{kPa}\cdot\mathrm{s}$, $\mu_{\mathrm{PMMA,10k}} \approx 14\,\mathrm{kPa}\cdot\mathrm{s}$ and $\mu_{\mathrm{PMMA,14k}} \approx 20\,\mathrm{kPa}\cdot\mathrm{s}$. The surface tension of PMMA in air is $\gamma_{\mathrm{PMMA/air}} = 33 \pm 3$ mN/m.

The used PMMA and PS polymers are all glassy at room temperature and their topography can be easily imaged by atomic force microscopy (AFM) Tapping Mode™ (Veeco, Santa Barbara, USA). PS revealed a contact angle on PMMA of $\vartheta_3 = 178.7 \pm 1^\circ$, see sketch in figure 1. Note, that in the considered case of dewetting on a deformable viscous substrate, the liquid/substrate interface is not constrained to a plane as it would be if it were dewetting on a rigid substrate, but adjusts itself to minimize the surface free energy, so that in equilibrium the condition (Neumann's triangle)

$$\begin{aligned} \gamma_{PS/air} + \cos(\vartheta_3)\gamma_{PMMA/air} + \cos(\vartheta_1)\gamma_{PS/PMMA} &= 0 \\ \gamma_{PMMA/air} + \cos(\vartheta_3)\gamma_{PS/air} + \cos(\vartheta_2)\gamma_{PS/PMMA} &= 0 \end{aligned}$$

with $\vartheta_1 + \vartheta_2 + \vartheta_3 = 2\pi$ holds true.

3 Theoretical model and numerical method

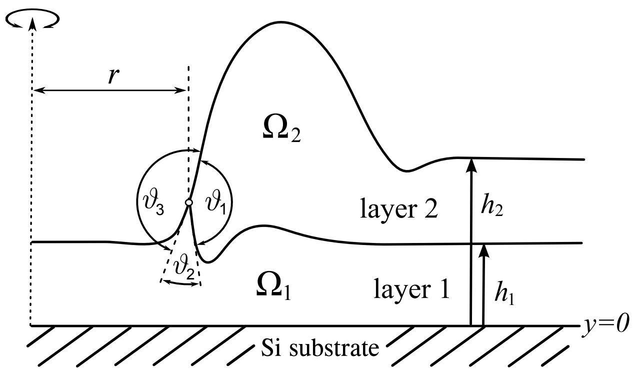

Figure 1: Sketch of the cross section of a dewetting liquid layer 2 (here PS) on another liquid layer 1 (here PMMA) on top of a silicon substrate. The growing hole above layer 1 has radius r. By h_i we denote the positions of the free interfaces above the substrate. The angles ϑ_i are spanned by the vectors tangential to the phase boundaries and normal to the three-phase contact line between PS, PMMA and air.

To theoretically describe the liquid/liquid dewetting process for the polymers that are used in the experiments and described in section 2, the governing equations for the bulk of both liquids occupying the region Ω_1 (PMMA), and occupying the region Ω_2 (PS), are the Navier-Stokes equations

$$\rho_i(\partial_t \mathbf{u}_i + \mathbf{u}_i \cdot \nabla \mathbf{u}_i) = \nabla \cdot \sigma_i + \mathbf{f}_i \quad \text{in} \quad \Omega_i\,, \quad i = 1, 2\,. \tag{1}$$

Figure 1 shows a sketch of a typical dewetting scenario after rupture of layer 2 (PS) from layer 1 (PMMA). The domains $\Omega_i\,, i = 1, 2$, where the solutions of (1) are defined, are given by

$$\Omega_1(t) = \left\{(r, y) \in \mathbb{R}^2 : 0 < y < h_1(t, r)\right\} \tag{2}$$
$$\Omega_2(t) = \left\{(r, y) \in \mathbb{R}^2 : h_1(t, r) < y < h_2(t, r)\right\} \tag{3}$$

The position of the Si-PMMA substrate is located at $\Gamma_0 = \{y = 0\}$, whereas the position of the PMMA/PS and PS/air interface located at $\Gamma_1 = \{y = h_1\}$ and $\Gamma_2 = \{y = h_2\}$, respectively.

The velocities during dewetting in each domain Ω_i are denoted by $\mathbf{u}_i$, the densities of PMMA and PS are denoted by ρ_i, $i = 1, 2$, respectively. Accordingly, the stress tensor for the two Newtonian fluids are

$$\sigma_i = -p_i \mathbb{I} + \mu_i (\nabla \mathbf{u}_i + \nabla \mathbf{u}_i^\top) \,, \quad i = 1, 2 \,, \tag{4}$$

where μ_i and p_i with $i = 1, 2$ denote the viscosities and pressure of PMMA and PS, respectively.

The equations in the two domains are coupled by a stress jump condition

$$(\sigma_2 - \sigma_1) \cdot \mathbf{n}_1 = -2\gamma_1 \kappa_1 \, \mathbf{n}_1 \tag{5}$$

at Γ_1, where $\mathbf{n}_1$ is a normal vector onto the boundary Γ_1, κ_1 is the mean curvature and γ_1 the coefficient for the surface tension between PS and PMMA. Furthermore we have a kinematic condition

$$(\partial_t h_1 \, \mathbf{j} - \mathbf{u}_1) \cdot \mathbf{n}_1 = 0 \tag{6}$$

at Γ_1, which fixes the normal component of the velocity of the interface; $\mathbf{j}$ is the unit vector $\mathbf{j} = (1, 0, 0)$. The velocity $\mathbf{u}_1$ is continuous across the interface Γ_1. At the interface Γ_2, we have the corresponding stress condition

$$-\sigma_2 \cdot \mathbf{n}_2 = -2\gamma_2 \kappa_2 \, \mathbf{n}_2 \tag{7}$$

and the kinematic condition

$$(\partial_t h_2 \, \mathbf{j} - \mathbf{u}_2) \cdot \mathbf{n}_2 = 0 \,. \tag{8}$$

The $\mathbf{f_i}$ that drive the dewetting denote the intermolecular forces and are given by the derivatives of the corresponding intermolecular potentials V_i, $i = 1, 2$. Typical choices for these potentials are composed of long-range van der Waals potentials together with short-range repulsion contributions, such as

$$V_2 = -V_1 = \frac{8\,|\phi^*|}{3} \frac{h^{*2}}{(h_2 - h_1)^3} - \frac{h^{*8}}{(h_2 - h_1)^9}, \tag{9}$$

see e.g. [5].

The characteristic length L of the evolving dynamic patterns are much larger in the lateral directions than the characteristic height H in the vertical direction. Hence

$$\varepsilon = \frac{H}{L} \ll 1 \tag{10}$$

emerges as a small parameter in the corresponding nondimensionalized problem. This allows an asymptotic reduction to leading order in ε, which results in the coupled system of thin film equations, given below. It constitutes a set of fourth-order partial differential equations for $h_1(r, t)$ and $h_2(r, t)$, that retain contributions arising from viscous dissipation, surface tension, and intermolecular forces. Moreover, since we will compare the profiles of the cross-sections of the free interfaces (PS/air and PMMA/PS) for single growing holes, we are only interested in axially symmetric solutions $h_1(r,t)$ and $h_2(r,t)$ so that we can use the corresponding versions of divergence and gradient. The system of thin film equations is therefore given by

$$\partial_t h_i = \mathrm{div} \sum_{j=1,2} Q_{ij}\ \mathrm{grad}\, \pi_j \tag{11}$$

where $i = 1, 2$ with

$$\pi_j = -2\, \tilde{\gamma}_j\, \kappa_j + V_j \tag{12}$$

where $j = 1, 2$ and model parameters

$$\tilde{\gamma}_1 = \gamma = \frac{\gamma_1}{\gamma_2}, \qquad \tilde{\gamma}_2 = 1. \tag{13}$$

The mean curvature is given by

$$2\kappa_j = \frac{\partial_r^2 h_j}{(1+\varepsilon^2(\partial_r h_j)^2)^{3/2}} + \frac{\partial_r h_j}{r\,(1+\varepsilon^2(\partial_r h_j)^2)^{1/2}} \tag{14}$$

For the corresponding symmetric mobility matrix $(Q_{ij})_{i,j=1,2}$ we then find for Q_{ij}

$$Q_{11} = \frac{1}{\alpha}\frac{h_1^3}{3} \tag{15}$$

$$Q_{12} = \frac{1}{\alpha}\frac{h_1^2}{2}\left(h_2 - \frac{h_1}{3}\right) = Q_{21} \tag{16}$$

$$Q_{22} = \frac{1}{\alpha}\left(\frac{(h_2-h_1)^3}{3}(\alpha-1) + \frac{h_2^3}{3}\right) \tag{17}$$

where

$$\alpha = \frac{\mu_1}{\mu_2} \tag{18}$$

denotes the relative viscosity of the PMMA phase with respect to the PS phase.

For the comparisons with the experimental result, we numerically solve equations (11) - (17) using a fully nonlinear implicit Euler method with adaptive time-stepping and adaptive finite differences in space, where the spatial resolution is increased near the contact line. For all simulations the initial conditions $0 < h_1(0,r) < h_2(0,r)$ were chosen such that $h_1(0,r) = H$ where $H = 200\,$nm, and $h_2(0,r)$ is a smooth step function with values $H + h^*$ for $r < 0.3\,\mu$m and $H + 35\,$nm, respectively $H + 50\,$nm for $r > 0.5\,\mu$m.

4 Results and Discussions

In order to induce dewetting, the PS/PMMA samples were annealed above the glass transition temperature of both polymers; for the presented quantitative result we used T = $170\,^{\circ}\mathrm{C}$. A time series of PS film dewetting from a liquid PMMA substrate is shown in Fig. 2. After a few minutes of annealing, circular holes appear on the PS film and their radii r grow with time.

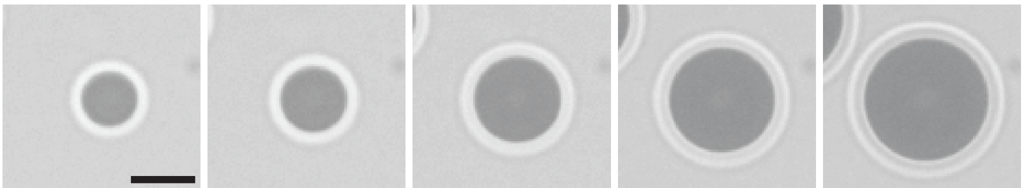

Figure 2: Time series of a dewetting hole of PS (17k) on PMMA (10k) at T$= 160°$C, shown 30, 40, 55, 65, and 80 seconds after rupture. The black bar corresponds to 50 μm.

For identical experimental conditions the dewetting rates found for different holes are identical within experimental errors. Thus in Fig. 3 (top) we only show one example for every considered experimental condition. Within the plotted range of radii, the hole growth follows approximately a linear law. However, a deviation from this linear behavior might occur for hole radii below 5 μm, as found e.g. for the dewetting dynamics of certain polymers on solid substrates, see [30], but this cannot be determined with our present experimental resolution.

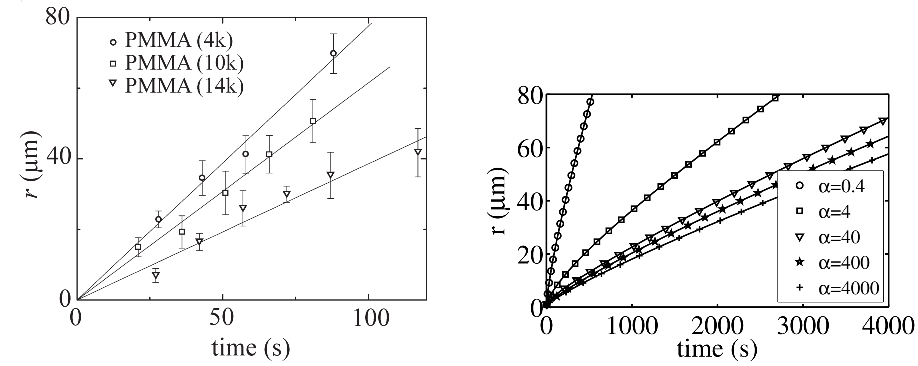

Figure 3: *Top:* Experimentally determined dewetting rates of a $50\,nm$ PS (17k) film dewetting at 170 $°\mathrm{C}$ on PMMA substrates of different molecular weights; PMMA (4k) (open circles, $\alpha \approx 30$); PMMA (10k) (open squares, $\alpha \approx 50$); PMMA (14k) (open triangles, $\alpha \approx 100$). r denotes the radius of the hole, whereas the time is the dewetting time measured from the extrapolated hole break up. *Bottom:* Numerically obtained dewetting rates for $\alpha = 0.4$ (open circles), $\alpha = 4$ (open squares), $\alpha = 40$ (open triangles); $\alpha = 400$ (solid stars), and $\alpha = 4000$ (crosses).

We observe in Fig. 3 that the dewetting rates decrease as the substrate molecular weight, and thereby the substrate viscosity, increases. Our numerical simulations of the dewetting rates are consistent with this experimentally observed trend for the considered range of low molecular weights of the PMMA substrate. Starting the simulations at very small hole radii, we find an decreasing dewetting velocity within the first micrometers of hole radii. For larger hole radii the velocity settles as constant, i.e $r \sim t$, in agreement with experimental data. However, the experimentally determined dewetting velocity is about one order of magnitude larger than the experimentally determined dewetting rate. This might be mainly due to uncertainties in the experimental viscosity ratio which are within the same order and uncertainties in the contact angles, or equivalently spreading coefficient which are both difficult to determine experimentally with the required precision.

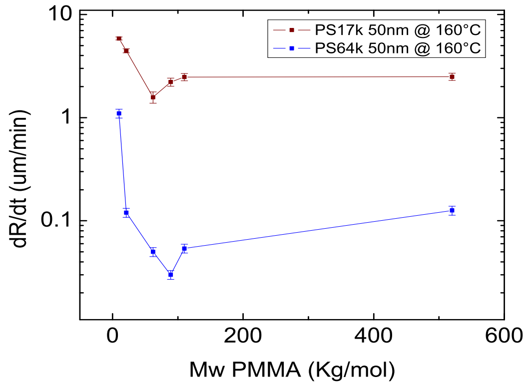

Figure 4: Dewetting rates as a function of PMMA chain lengths for PS (17k) (upper graph) and PS (64k) (lower graph) at T$= 160°$C

Interestingly, if we keep increasing the PMMA molecular weight, our experiments also show that a second regime appears, in which the dewetting rates increase with increasing molecular weight, and even a third regime appears where the dewetting rates are about independent of the molecular weight of the substrate. This is shown in Fig. 4 for the case of PS (17k) and PS (64k) and various PMMA substrates of increasing molecular weights. These results are not compared here, as they exceed the aim of this paper, but they are in good qualitative agreement with the findings of Lambooy et al. [31] and [21]. Since the second and third regime appear for larger molecular weights where elastic properties will significantly influence the dewetting scenario, these regimes will not be captured by our theoretical studies and simulations assuming a thin film model based on Newtonian rheology.

To further explore the process of a liquid film dewetting from a liquid substrate we also investigate the emerging rim profiles in particular their dependence on the substrate's viscosity. In our experiments we measured the PS rim profile after we stopped the dewetting experiment, and once a hole had reached the desired radius. This was done by quenching the sample to room temperature in order to cool both polymers below their respective glass transition temperature. In the glassy state the shape of the dewetting rims and the solidified substrate can be easily determined with great lateral precision using AFM in Tapping Mode. Previous experiments revealed that the shape of a formerly liquid structure is not changed by this quenching process within our experimental accuracy [14, 32]. To image also the deformation of the PS/PMMA interface, we removed the overlying PS film by a selective solvent (Cyclohexane) and subsequently imaged the remaining PMMA film. The PMMA film is glassy at room temperature and the shape of the former liquid/liquid interface is frozen into it, see in Fig. 5 (top) and Fig. 6 (top). To illustrate the dependence of the rim profile on hole radius and PMMA chain length, we compiled four experimentally determined rim profiles for two different PMMA molecular weights: PMMA (14k) see Fig. 5 (top) and PMMA (4k), see Fig. 6 (top). In each case we examined two hole radii, 4 μm and 10 μm. We point out that in Fig. 5 and Fig. 6, for better illustration, all graphs are "cut" at the height 100 nm from the surface of the silicon substrate.

For the more viscous substrate PMMA (14k) in Fig. 5 (top) the shape of the PS/PMMA interface

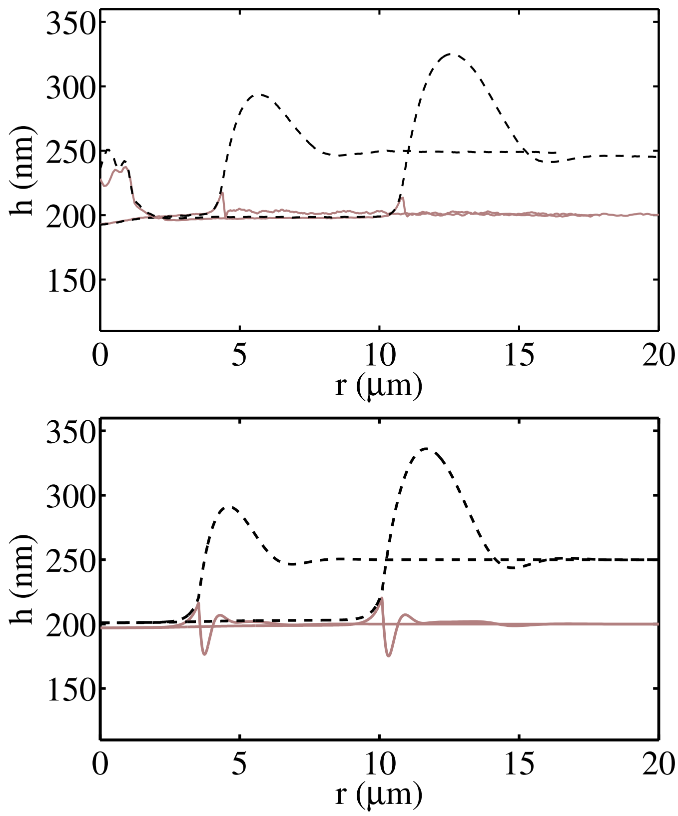

Figure 5: *Top:* Experimental results of the PS/air and PS/PMMA interface deformations of a growing hole of a 50 nm PS (17k) film dewetting at 170 $^\circ\mathrm{C}$ from a 200 nm PMMA (14k) layer. The experimental viscosity ratio is $\alpha \approx 100$ *Bottom:* Numerical solution of (11)-(17) for simulation parameters $\alpha = 400$ and $\gamma = 0.2$.

is only slightly deformed. Even for longer time intervals when the dewetting front has reached approximately 10 μm the growth occurs rather in the lateral direction than in the vertical direction. The typical shapes show a ridge followed by a dip and a very shallow hump that decays toward the undisturbed film. The height of the dewetted and undisturbed PMMA (14k) layer remains about the same. The experimental rim profiles do not visibly vary over various experimental runs, and can be overlaid for identical experimental parameters. Only the disturbance and the possible resulting deformation of the PMMA/air interface at $r = 0$, i.e. the center of the hole, should be disregarded. These are very likely remains from physical heterogeneities which initiated the hole rupture by heterogeneous nucleation and vary from hole to hole without influencing the dewetting velocity and the shape of the rim profile.

In contrast, in the case of less viscous substrates, where the height of the dewetted PMMA (4k) layer is considerably decreased (see Fig. 6, middle and bottom) and transported by the dewetting rim in direction of the undisturbed film. Hence the amplitude of the depression right before the contact line strongly depends on the viscosity of the underlying PMMA layer.

The height of the ridge and the dip behind the dewetting front is larger in case of the softer PMMA substrate. The hump behind the dip is considerably larger and grows in height and in

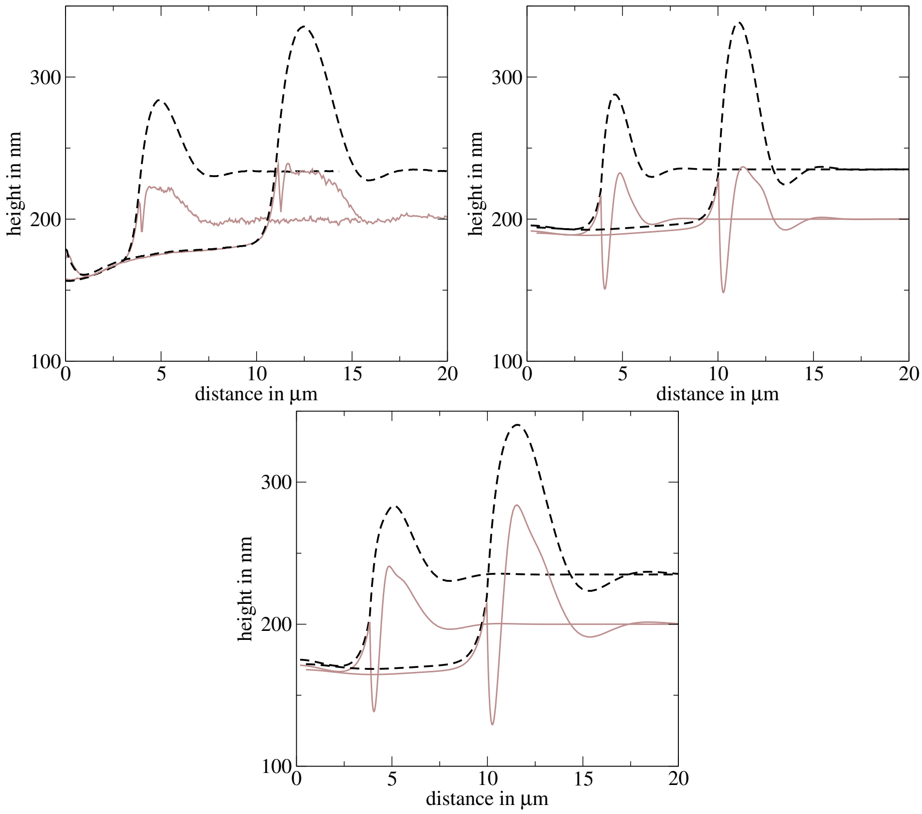

Figure 6: *Top:* Experimental results of the PS/air and PS/PMMA interface deformations of a growing hole in a 35 nm thick PS (17k) film dewetting at 170 $^{\circ}\mathrm{C}$ from PMMA (4k). The experimental viscosity ratio is $\alpha \approx 30$. *Middle:* Numerical solution of (11)-(17) for simulation parameters $\alpha = 40$ and $\gamma = 0.2$. *Bottom:* Numerical solution for simulation parameters $\alpha = 4$ and $\gamma = 0.2$.

width in accordance with the growing PS rim, suggesting that the removed PMMA substrate material accumulates below the bulged part of the PS rim. This effect is more pronounced for lower PMMA chain length indicating that the tangential forces at the contact line acting parallel to the liquid/liquid interface are more important in this case. The shape of this hump develops a slight plateau.

We also note that the size of the PS rim and succeeding depression is reduced for faster dewetting velocities, i.e. larger PMMA chain length in our case, which agrees with the finding on solid substrates [14, 32].

For comparison of the calculated results with the experimental results, we used the experimental parameters, respectively, the parameters derived from our experiments such as surface energies, viscosities, contact angle and film heights as input parameter to the numerical calculation. It is worth mentioning that the experimental uncertainties of these values are significant, in particular since the ratios of these values, i.e. the ratios of PMMA/air and the PS/air surface tension, and viscosity enter the numerical simulation. The numerically obtained interface profiles are displayed in Fig. 5 (bottom) and Fig. 6 (middle and bottom).

In order to compare the experimental interface profiles h_1 and h_2 with our model, we have chosen initial conditions corresponding to the undisturbed liquid/liquid system with a slight corrugation at $r = 0$ in form of a smoothed shock for the PS layer. In contrast to the experimental profiles the deviations near the origin does not appear, since this is due to the actual rupture event, which we do not model here. We have chosen the surface tension $\gamma_{\mathrm{PMMA/PS}}$ and $\gamma_{\mathrm{PS/air}}$ within the uncertainties of the experimentally obtained values, and matched the spreading coefficient $\gamma = \gamma_{\mathrm{PMMA/air}} - \gamma_{\mathrm{PMMA/PS}} - \gamma_{\mathrm{PS/air}}$ to obtain similar contact angles as the ones observed in the experiment. To see what the effect of changing the PMMA-viscosity is, we varied α over several orders of magnitude. We chose $\gamma = 0.2$ and varied the viscosity contrast between $\alpha = 40$ to $\alpha = 400$.

Within the chosen parameter range, the best matches of numerical and experimental data were achieved for $\alpha = 400$ in Fig. 5 and $\alpha = 40$ in Fig. 6. These viscosity ratios are within the experimental values $\alpha \approx 100$ and $\alpha \approx 30$. Please note that for experimental reasons each viscosity is not better defined than about a factor of three, leading to an uncertainty of about one order of magnitude for the viscosity ratio α. The achieved agreement of the rim proffiles is satisfactory but we still find systematic differences. The most obvious one is that the sharp dip in the PS/PMMA interface right before the three phase contact line is more pronounced in the numerically determined rim profiles than in the experimentally determined rim profiles. A likely reason for this difference might be either that the experimental value of the interfacial energy of the PS/PMMA interface is higher than assumed or that the contact angle is slightly different. For this reason all experimental values taken from literature will have to be revisited carefully.

5 Conclusions

We have carried out a systematic study and compared experimental and theoretical results of a dewetting thin PS film on liquid PMMA substrates, as a function of the substrate viscosity properties. Both polymers were kept below their entanglement lengths and were modeled as Newtonian liquids. We have shown that the dewetting rates increase for substrates of higher viscosity, an observation that coincides with an increasing deformation of the liquid/liquid interface. The numerically derived rim shapes and dewetting behavior match the these trends as well as the corresponding qualitative interface profiles found in our experiments. Further experimental work will be needed to narrow the uncertainties of the values for interfacial tensions. Also, theoretical work will include viscoelastic properties of the substrate to compare with experimental findings of Krausch et al. [19, 20] and our results, as shown in Fig. 4.

References

[1] L. Leger and J. F. Joanny. Liquid spreading. *Reports on Progress in Physics*, 55(4):431–486, 1992.

[2] S. Herminghaus. Dynamical instability of thin liquid films between conducting media. *Physical Review Letters*, 83(12):2359, 1999.

[3] R. Seemann, S. Herminghaus, and K. Jacobs. Gaining control of pattern formation of dewetting liquid films. *Journal of Physics: Condensed Matter*, 13(21):4925–4938, 2001.

[4] G. Reiter. Dewetting of thin polymer films. *Physical Review Letters*, 68(1):75–78, 1992.

[5] R. Seemann, S. Herminghaus, and K. Jacobs. Dewetting patterns and molecular forces: A reconciliation. *Physical Review Letters*, 86(24):5534–5537, 2001.

[6] M. B. Williams and S. H. Davis. Nonlinear theory of film rupture. *Journal of Colloid Interface Science*, 90:220–228, 1982.

[7] K. Jacobs, S. Herminghaus, and K.R. Mecke. Thin liquid polymer films rupture via defects. *Langmuir*, 14(4):965–969, 1998.

[8] F. Brochard-Wyart, G. Debregeas, R. Fondecave, and P. Martin. Dewetting of supported viscoelastic polymer films: Birth of rims. *Macromolecules*, 30(4):1211–1213, 1997.

[9] J.-L. Masson and P.F. Green. Hole formation in thin polymer films: a two-stage process. *Physical Review Letters*, 88(20):205504, 2002.

[10] F. Brochard-Wyart and P.G. de Gennes. Shear-dependent slippage at a polymer/solid interface. *Langmuir*, 8:3033–3037, 1992.

[11] A. Münch, B. Wagner, and T. P. Witelski. Lubrication models with small to large slip lengths. *Journal of Engineering Mathematics*, 53:359–383, 2006.

[12] C. Neto and K. Jacobs. Dynamics of hole growth in dewetting polystyrene films. *Physica A: Statistical Mechanics and its Applications*, 339(1-2):66–71, 2004.

[13] R. Fetzer, M. Rauscher, A. Münch, B. A. Wagner, and K. Jacobs. Slip-controlled thin-film dynamics. *Europhysics Letters*, 75(4):638–644, 2006.

[14] R. Seemann, S. Herminghaus, and K. Jacobs. Shape of a liquid front upon dewetting. *Physical Review Letters*, 87:196101, 2001.

[15] A. M. Higginsa, M. Sferrazza, R. A. L. Jones, P.C. Jukes, J.S. Sharp, L. E. Dryden, and J. Webster. The timescale of spinodal dewetting at a polymer/polymer interface. *The European Physics Journal E: Soft Matter*, 8:137–143, 2002.

[16] J.P. de Silva, M. Geoghegan, A.M. Higgins, G. Krausch, M.O. David, and G. Reiter. Switching layer stability in a polymer bilayer by thickness variation. *Physical Review Letters*, 98(26):267802, 2007.

[17] R.A. Segalman and P.F. Green. Dynamics of rims and the onset of spinodal dewetting at liquid/liquid interfaces. *Macromolecules*, 32(3):801–807, 1999.

[18] D. Slep, J. Asselta, M. H. Rafailovich, J. Sokolov, D. A. Winesett, A. P. Smith, H. Ade, and S. Anders. Effect of an Interactive Surface on the Equilibrium Contact Angles in Bilayer Polymer Films. *Langmuir*, 16:2369–2375, 2000.

[19] P. Lambooy, K.C. Phelan, O. Haugg, and G. Krausch. Dewetting at the liquid-liquid interface. *Physical Review Letters*, 76(7):1110–1113, 1996.

[20] C. Wang, G. Krausch, and M. Geoghegan. Dewetting at a Polymer-Polymer Interface: Film Thickness Dependence. *Langmuir*, 17(20):6269–6274, 2001.

[21] F. Brochard Wyart, P. Martin, and C. Redon. Liquid/liquid dewetting. *Langmuir*, 9(12):3682–3690, 1993.

[22] S. Qu, C. J. Clarke, Y. Liu, M. H. Rafailovich, J. Sokolov, K. C. Phelan, and G. Krausch. Dewetting dynamics at a Polymer-Polymer interface. *Macromolecules*, 30(12):3640–3645, 1997.

[23] A. Pototsky, M. Bestehorn, D. Merkt, and U. Thiele. Alternative pathways of dewetting for a thin liquid two-layer film. *Physical Review E*, 70(2):25201, 2004.

[24] A. Pototsky, M. Bestehorn, D. Merkt, and U. Thiele. Morphology changes in the evolution of liquid two-layer films. *The Journal of Chemical Physics*, 122:224711, 2005.

[25] L.S. Fisher and A.A. Golovin. Nonlinear stability analysis of a two-layer thin liquid film: Dewetting and autophobic behavior. *Journal of Colloid and Interface Science*, 291(2):515–528, 2005.

[26] L.S. Fisher and A.A. Golovin. Instability of a two-layer thin liquid film with surfactants: Dewetting waves. *Journal of Colloid and Interface Science*, 307(1):203–214, 2007.

[27] D. Bandyopadhyay, R. Gulabani, and A. Sharma. Instability and dynamics of thin liquid bilayers. *Industrial and Engineering Chemistry Research*, 44(5):1259–1272, 2005.

[28] D. Bandyopadhyay and A. Sharma. Nonlinear instabilities and pathways of rupture in thin liquid bilayers. *The Journal of Chemical Physics*, 125:054711, 2006.

[29] R. Fetzer and K. Jacobs. Slippage of newtonian liquids: Influence on the dynamics of dewetting thin films. *Langmuir*, 23(23):11617–11622, 2007.

[30] K. Jacobs, R. Seemann, G. Schatz, and S. Herminghaus. Growth of holes in liquid films with partial slippage. *Langmuir*, 14:4961–4963, 1998.

[31] P. Lambooy, K. C. Phelan, O. Haugg, and G. Krausch. Dewetting at the liquid-liquid interface. *Physical Review Letters*, 76(7):1110, 1996.

[32] R. Fetzer, K. Jacobs, A. Münch, B. Wagner, and T.P. Witelski. New slip regimes and the shape of dewetting thin liquid films. *Physical Review Letters*, 95(12):127801, 2005.